Simulation of transient fluid flow in mold region during steel continuous casting

R Liu[1], B G Thomas[1], and J Sengupta[2]

[1] Department of Mechanical Science and Engineering, University of Illinois at Urbana-Champaign, 1206 West Green Street, Urbana, IL, 60801, USA
[2] ArcelorMittal Global R&D Hamilton, ArcelorMittal Dofasco Inc., 1390 Burlington Street East, Hamilton, ON, L8N 3J5 Canada

E-mail: bgthomas@illinois.edu, and joydeep.sengupta@arcelormittal.com

Abstract. A system of models has been developed to study transient flow during continuous casting and applied to simulate an event of multiple stopper-rod movements. It includes four sub-models to incorporate different aspects in this transient event. A three-dimensional (3-D) porous-flow model of the nozzle wall calculates the rate argon gas flow into the liquid steel, and the initial mean bubble size is estimated. Transient CFD models simulate multiphase flow of steel and gas bubbles in the Submerged Entry Nozzle (SEN) and mold and have been validated with experimental data from both nail dipping and Sub-meniscus Velocity Control (SVC) measurements. To obtain the transient inlet boundary conditions for the simulation, two semi-empirical models, a stopper-rod-position based model and a metal-level-based model, predict the liquid steel flow rate through the SEN based on recorded plant data. Finally the model system was applied to study the effects of stopper rod movements on SEN/mold flow patterns. Meniscus level fluctuations were calculated using a simple pressure method and compared well with plant measurements. Insights were gained from the simulation results to explain the cause of meniscus level fluctuations and the formation of sliver defects during stopper rod movements.

1. Introduction

Continuous casting is the predominant way of steel-producing. During this process, liquid steel flows from the tundish bottom, through the upper tundish nozzle (UTN), and submerged entry nozzle (SEN), and jets from the bifurcated ports near the SEN bottom into the water-cooled mold where a solid shell of steel solidifies to contain the liquid pool. Argon gas is injected through the porous refractory walls of the UTN in order to prevent nozzle clogging and reoxidation. It forms gas bubbles, which greatly affect the flow pattern in the mold and also help to remove some inclusions by floating them to the liquid flux layer. Flow rate is controlled by vertical motion of a stopper rod into the top of the UTN. The liquid steel jets from the nozzle carry nonmetallic inclusions from upstream into the liquid steel pool. Mold powder melts into liquid flux on the top surface of the liquid steel pool, which helps to prevent oxidation, as shown in Figure 1 [1]. Liquid slag may be entrained into the liquid steel pool via various mechanisms, as summarized by Hibbeler and Thomas [2]. Some of the inclusion particles, slag droplets and argon bubbles which touch the solidifying shell may become entrapped into the solidifying shell, and become defects in the final product. The flow of steel in the liquid pool has a huge impact on the transport and entrapment of inclusions, but genuine transient events have received little study.

In the current work, a transient event with multiple stopper rod movements at ArcelorMittal Dofasco's No.1 continuous caster is investigated via numerical simulation. The recorded histories of the stopper rod position and meniscus level in Figure 2 [3] show sudden movements of the stopper rod and intensive fluctuations of the meniscus level, accompanying a nearly constant casting speed. Sliver images and locations were obtained and analyzed from the downstream coil samples, and a defect was identified to be caused by the multiple stopper rod movements.

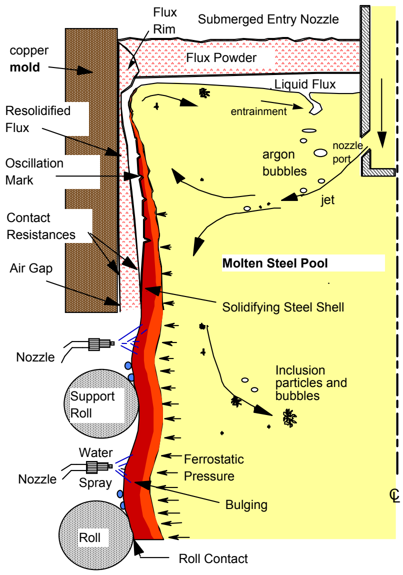

Figure 1. Complex transport processes in mold region [1]

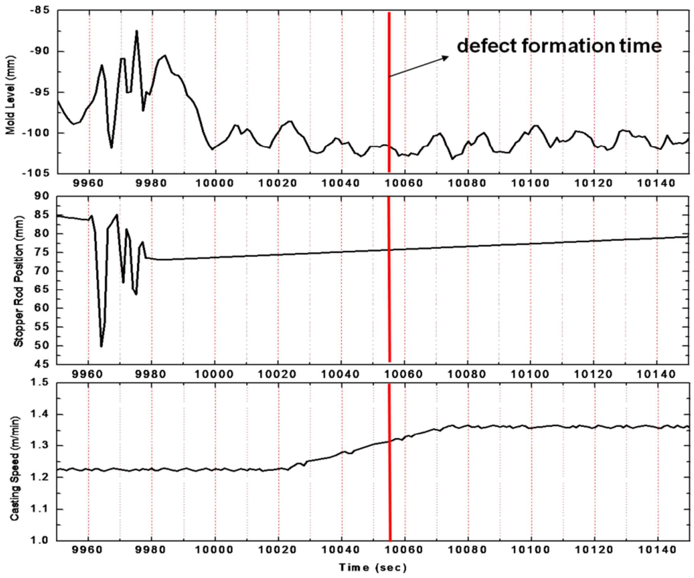

Figure 2. Recorded stopper rod position, mold level and casting speed [3]

Four sub-models were developed to incorporate the different aspects of this complex problem. Each sub-model has been validated independently using plant/lab measurements. Then, the complete model system is applied to simulate the transient multiphase flow phenomena during this process, and the mechanism for the defect formation during this process is discussed.

2. Model Description and Validation

The complete model system for this transient simulation consists of 1) a porous-flow model to study gas flow through heated UTN refractory as well as initial mean bubble size at UTN inner surface, 2) a stopper-position-based model, 3) a metal-level-based model to predict liquid steel flow rate inside SEN during stopper rod movements which is required as boundary condition for the two-phase flow simulations, and 4) an Eulerian-Mixture CFD model to simulate argon-steel two-phase flow in the nozzle and mold region, and a pressure-based post-processing method to estimate meniscus level.

2.1. Porous-flow model of argon gas in nozzle wall

Argon gas is injected into the lower part of the UTN, through grooves and slits to distribute it around the nozzle refractory. Applied back pressure forces the argon to diffuse through the porous refractory walls to form bubbles when it exits from the tiny pore openings, (active sites) at the UTN inner surface, as shown in the schematic in Figure 3. This injected argon gas significantly influences liquid steel flow in the nozzle and mold region. Two key parameters required to simulate argon-steel two phase flows are the gas flow rate and the initial bubble size injected into the steel. In this work, a new porous-flow model was developed, combined with other models, validated and applied to determine these two parameters for the subsequent transient flow simulations.

The “cold” argon flow rate is measured at standard temperature and pressure (STP) before entering the nozzle. This flow rate is much smaller than the “hot” argon flow rate, due to its great thermal expansion upon entering the liquid steel. To determine this flow rate, a heat transfer analysis was first performed to obtain the temperature distribution across the UTN wall.

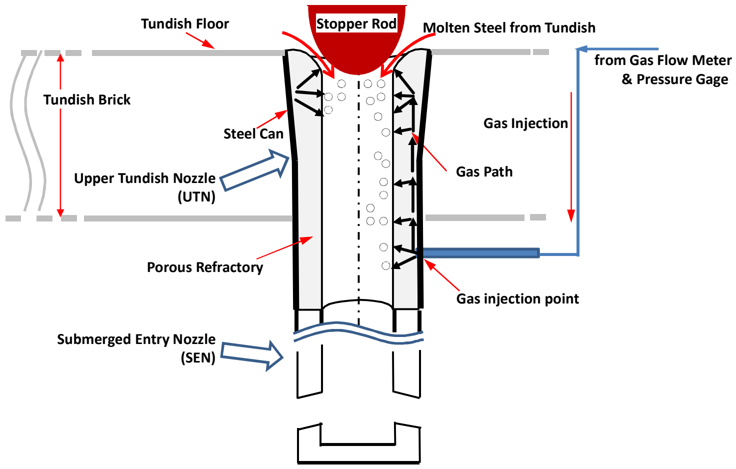

Figure 3. Schematic of gas bubble formation locations from UTN surface (slits not shown)

Then, Equation (1) is solved for the pressure distribution. It is derived from the continuity equation, Darcy’s law, and the ideal gas law, to incorporate the effects of pressure and temperature on the gas volume [4]. The effect of gas viscosity change with temperature on refractory permeability K_D is considered using the viscosity-temperature correlation by Dawe [5].

$$\nabla \cdot (K_D \nabla p) = -\frac{RT}{p}\left[\nabla\left(\frac{p}{RT}\right)\cdot(K_D \nabla p)\right] \tag{1}$$

Next, the gas velocity distribution exiting the UTN surface is computed from Darcy’s law via user-defined functions (UDF) with commercial CFD package FLUENT [6], distributed by ANSYS, Inc. The initial mean bubble size is then estimated, based on this velocity distribution and the corresponding number of active sites from the empirical correlation by Lee [7], using the semi-analytical two-stage model for predicting bubble size in downward cross-flow from Bai [8]. Details on the steps to estimate initial mean bubble size can also be found in [4].

To validate the porous-flow model, a static test was performed using a real UTN from ArcelorMittal Dofasco’s No. 1 CC, which was cut in half, sealed at the cut surface, and placed in a water tank. Air was injected through the input hose connected to the outer wall and the locations of bubbles emerging from the inner wall are photographed in Figure 4a). The locations are compared with the preferential bubble locations predicted by the porous flow model, as indicated in Figure 4b) via the gas velocity distribution. Regions of higher gas velocity generate more and larger bubbles [8].

Note that the UTN in this experiment was cut in half along a plane perpendicular to the half-nozzle domain used in the simulation. Because of the good wetted condition between UTN refractory and water, the hydraulic pressure inside the nozzle, and capillary effects, water can enter some of the pores at the UTN inner surface and block the pore exits entirely. Thus, a threshold exists to prevent bubbles from exiting regions of low back pressure. During the experiment, back pressure was increased slowly, so the gas flow rate increased gradually from zero. The porous-flow model predicts a very non-uniform distribution of air velocity over the UTN inner surface, in Figure 4(b). Local pressure at the lowest-velocity locations was likely insufficient to overcome the threshold. It is important to note that the regions where no bubbles are observed in Figure 4(a) match well with the regions of low predicted gas velocity in Figure 4(b). Similarly, the high-velocity regions match with regions where large bubbles were observed. Thus a reasonable match was found between the simulation and experimental observations.

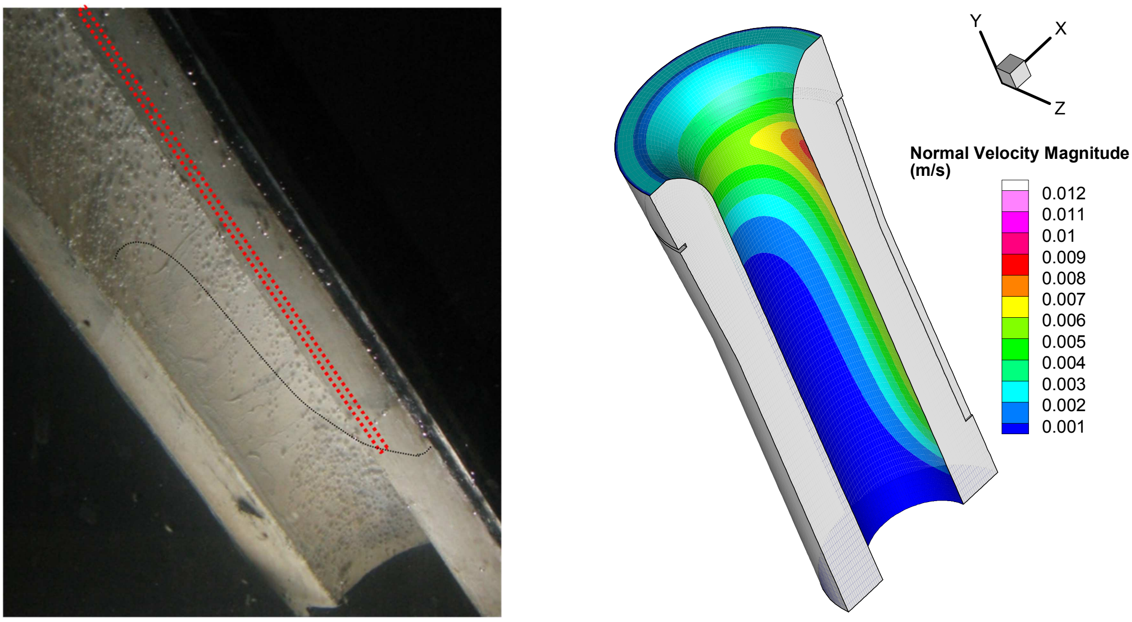

(a) Observed preferential bubbling locations (b) Predicted gas velocity distribution

Figure 4. Comparison between predicted and observed bubbling sites at UTN inner surface

2.2. Stopper-position-based model of SEN steel flow rate

During steady-state continuous casting, the liquid steel flow rate in the SEN equals the throughput at mold exit. During a transient event, however, steel flow rate in the SEN varies with time, as indicated by the rapid fluctuations of the average meniscus level. Two different models were developed in this work to predict the liquid steel flow rate into the SEN.

Firstly, a semi-analytical model, given in Equation (2), is derived from Bernoulli's equation to predict flow rate based on the measured stopper rod opening position and other parameters [3]. It is validated with plant measurements, as shown in Figure 5.

$$Q_{SEN} = A_{SEN}\left(\frac{2g\left(f_{tundish}h_{tundish} - h_{sen\_sub} + L_{SEN}\right)}{1+0.5\left(\frac{A_{SEN}}{C_2 h_{SRO}^2}\right)^2 + \left(\frac{A_{SEN}}{C_2 h_{SRO}^2} - 1\right)^2 + C_1\frac{L_{SEN}}{D_{SEN}} + C_3}\right)^{0.5} \quad (2)$$

In this equation, A_{SEN} is the SEN inner bore cross-section area; h_{sen_sub} is the submergence depth of SEN, $h_{tundish}$ is the total height of the tundish; $f_{tundish}$ is the tundish weight fraction; L_{SEN} is the total length of SEN; D_{SEN} is the SEN inner bore diameter; h_{SRO} is the stopper rod opening. The three parameters in the equation, C_1, C_2 and C_3, are adjustable coefficients that represent different pressure head losses: C_1 is for friction, C_2 is for the stopper rod gap and C_3 is for clogging. The influence of C_2 and C_3 on the predicted relation between stopper rod position and flow rate is shown in Figure 5(a) and 5(b) . The effect of argon gas injection on the pressure head loss at the stopper rod gap is accounted for in C_2. In this work, C_2 was calibrated using the plant trial data in Figure 5(a), which had the same gas volume fraction as in the current transient study (10% gas). The effect of friction factor on this relation is negligible.

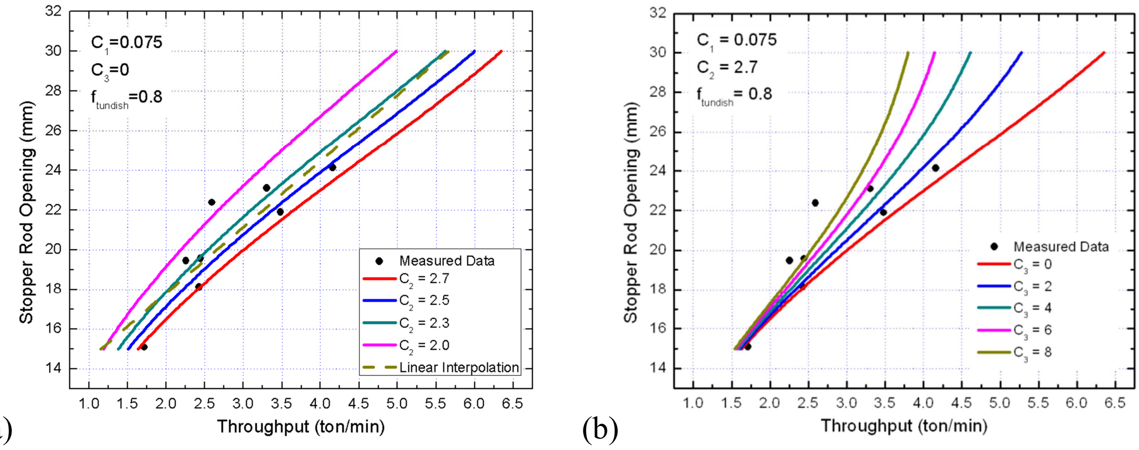

Figure 5. Effect of C_2 and C_3 on stopper-position-based model predictions of flow rate [3]

2.3. Metal-level-based model of SEN steel flow rate

A metal-level-based model was derived to predict flow rate based on an overall mass conservation of the system. Knowing the casting speed, the time variations of the liquid steel flow rate in the SEN are reflected in variations of the average position of the meniscus level. Using the recorded meniscus level and casting speed in the plant, the SEN flow rate can be approximated by Equation (3) [3].

$$Q_{SEN} = \frac{h_m(i+1) - h_m(i-1)}{2\Delta t}\left(W \cdot T - \frac{\pi d_{SEN,outer}^2}{4}\right) + V_{cast}(i) \cdot W \cdot T \tag{3}$$

In this equation, the index i represents the current time; Δt is the time step size, $V_{cast}(i)$ is the casting speed at time i; W is the mold width, T is the mold thickness; h_m is the measured meniscus level at time i; and $d_{sen,outer}$ is the SEN outer bore diameter. The measured meniscus location, midway across the mold, is assumed to be representative of the average liquid level in the mold.

2.4. Multiphase fluid flow model

Argon-steel two-phase flow in the nozzle and mold was simulated with a 3-D Eulerian-Mixture model, which solves for the mass and momentum conservation equations of the argon-steel mixture phase. The continuity equation of the mixture is shown in equation (4) and (5), and the momentum conservation equation is in equation (6).

$$\frac{\partial \rho_m}{\partial t} + \nabla \cdot (\rho_m \mathbf{u}_m) = 0 \tag{4}$$

$$\text{where } \mathbf{u}_m = \frac{\alpha_s \rho_s \mathbf{u}_s + \alpha_a \rho_a \mathbf{u}_a}{\rho_m}, \text{ and } \rho_m = \alpha_s \rho_s + \alpha_a \rho_a \tag{5}$$

$$\frac{\partial(\rho_m \mathbf{u}_m)}{\partial t} + \nabla \cdot (\rho_m \mathbf{u}_m \mathbf{u}_m) = -\nabla p + \nabla \cdot \left[\mu_m \left(\nabla \mathbf{u}_m + (\nabla \mathbf{u}_m)^T\right)\right] + \rho_m \mathbf{g} + \nabla \cdot (\alpha_a \rho_a \mathbf{u}_{dr,a} \mathbf{u}_{dr,a}) \tag{6}$$

The variables α_a and α_s represent the volumetric fractions of argon phase and liquid steel phase respectively, which are found by solving equation (7), and knowing that α_a and α_s sum to 1.

$$\frac{\partial(\alpha_a\rho_a)}{\partial t}+\nabla\cdot(\alpha_a\rho_a\mathbf{u}_m)=-\nabla\cdot(\alpha_a\rho_a\mathbf{u}_{dr,a}) \tag{7}$$

Drift velocity $\mathbf{u}_{dr,a}$ on the right hand side of equation (6) and equation (7) is defined in equation (8).

$$\mathbf{u}_{dr,a}=\mathbf{u}_{as}-\frac{\alpha_a\rho_a}{\rho_m}\mathbf{u}_{as}\text{, where the relative velocity is }\mathbf{u}_{as}=\mathbf{u}_a-\mathbf{u}_s \tag{8}$$

The mixture model is then closed using an algebraic slip formulation for the relative velocity $\mathbf{u}_{as}$ assuming that local equilibrium between phases is reached over a short spatial length, as shown in equation (9) [6], where the drag function f_{drag} is taken from Schiller and Naumann [9], and d_a is the argon bubble diameter. The standard k-ε model was applied to model turbulence in the mixture phase.

$$\mathbf{u}_{as}=\frac{(\rho_a-\rho_m)d_a^2}{18\mu_s f_{drag}}\left(\mathbf{g}-(\mathbf{u}_m\cdot\nabla)\mathbf{u}_m-\frac{\partial\mathbf{u}_m}{\partial t}\right) \tag{9}$$

The computational domain includes the nozzle and the liquid pool in the mold region, with the solidification front interface as the domain boundary. No-slip wall boundary condition is adopted at mold top surface, as the sintered slag layer serves as a solid wall. Mass and momentum sinks [10] are imposed at the layer of computational cells next to the shell boundary, to account for the liquid steel crossing the boundary due to solidification. Similar mass and momentum sinks are applied to quantify the argon gas escaping from the top surface. This model has been validated with extensive plant measurements using both the simple but powerful nail-dipping method and measurements using a Sub-meniscus Velocity Control (SVC) device. These two different measurement methods validate each other, based on their agreement in plant trials such as shown in Figure 6 [11].

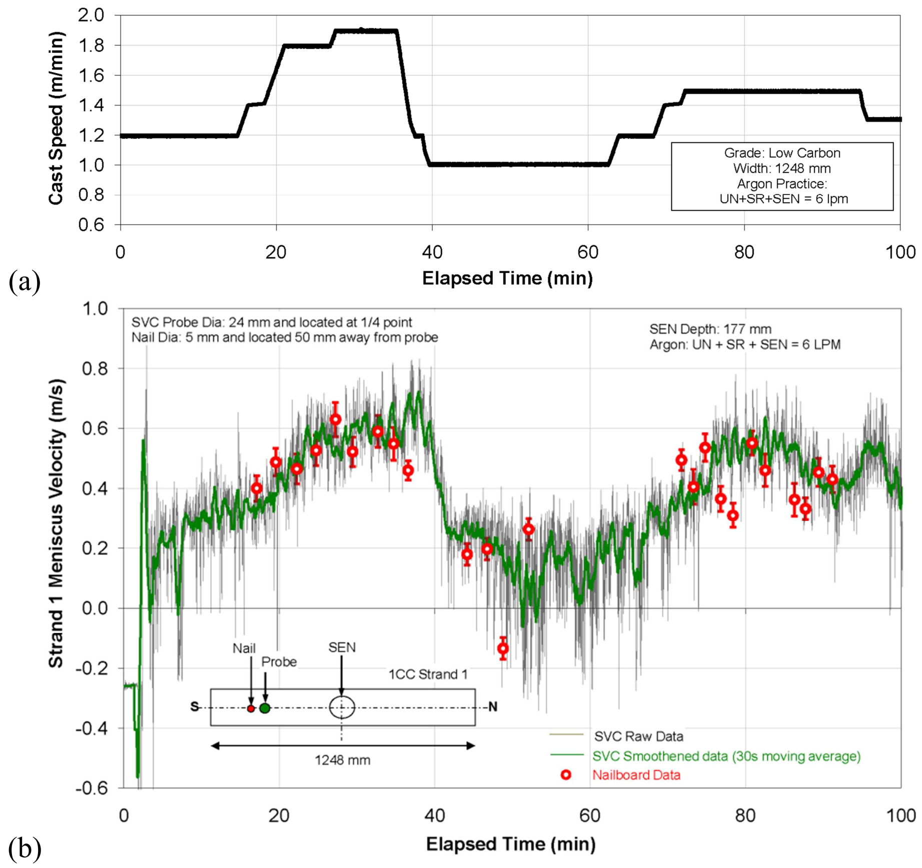

Figure 6. Plant trial comparing two surface velocity measurement methods [11]
(a) Casting speed history; (b) Meniscus velocity history from SVC and nail dipping tests.

One quarter of the SEN and mold were chosen as the computational domain for the validation cases [3]. Figure 7 shows the geometry and mesh of ~0.23 million hexahedral structured cells. The Dofasco No. 1 caster was 225mm thick with a bifurcated SEN with 15-deg downward ports, described elsewhere [3]. Three cases were simulated with Argon flow rate fixed at 6 SLPM, width of 983mm, submergence depth of 186mm, 2.5m long domain, and casting speeds of 1.5, 1.7 and 1.9 m/min. The calculated surface velocities are compared with results of the plant nail dipping tests in Figure 8. A reasonable match is obtained, which tends to validate the model. These results also confirm that increasing gas volume fraction (by decreasing casting speed), tends to change the double-roll flow pattern into a complex flow pattern, as expected from the water model results. Velocities near the SEN are directed towards the narrow face, opposing the classic surface flow towards the SEN. This reverse flow near the SEN is caused by liquid dragged upward there by the rising bubbles.

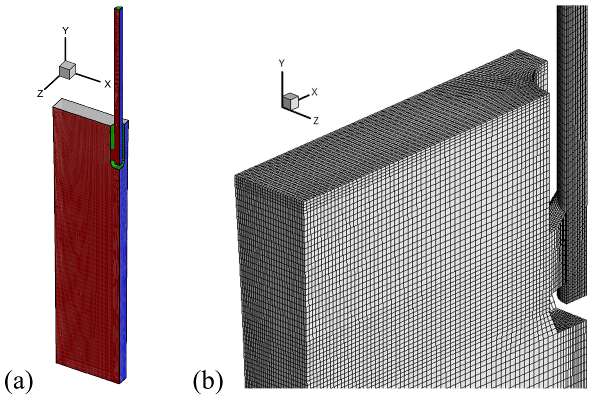

Figure 7. Computational domain geometry and mesh [3]

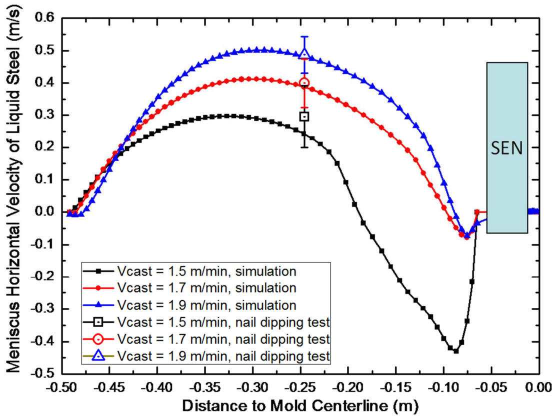

Figure 8. Comparison between predicted and measured surface velocities [3]

3. Results and Discussions

The system of models is applied to simulate the transient event described previously. The two semi-empirical models, stopper-position-based model and metal-level-based model, are used to generate the history of SEN inlet velocity boundary condition; then the porous-flow model was utilized to calculate the argon flow rate entering the UTN in hot condition, and bubble size was estimated; the transient two-phase flow simulation was run with Eulerian-Mixture model. Finally, the computed pressure at meniscus was converted to predict mold level, and compared with the measurements. The mesh consists of 0.8 million hexahedral cells in total, and time step size was 0.01sec. No-slip wall is adopted as the boundary condition at mold top surface, as the sintered slag layer serves as a solid wall.

3.1. Predicted SEN inlet liquid steel flow rate

The flow rate of the liquid steel in the SEN predicted by the stopper-position-based model and the metal-level-based model are compared in Figure 9. Note that translating the metal-level-based results back in time by 1.2sec (dashed line in Figure 9) makes the two predicted curves roughly match. This time interval represents the time delay for the steel to flow from the stopper into the mold. The SEN flow rate from stopper-position-based model is adopted in the subsequent simulation. A major flow rate drop occurred around 9965sec, and the corresponding flow pattern changes between 9955 and 9971.7sec are investigated in the following section.

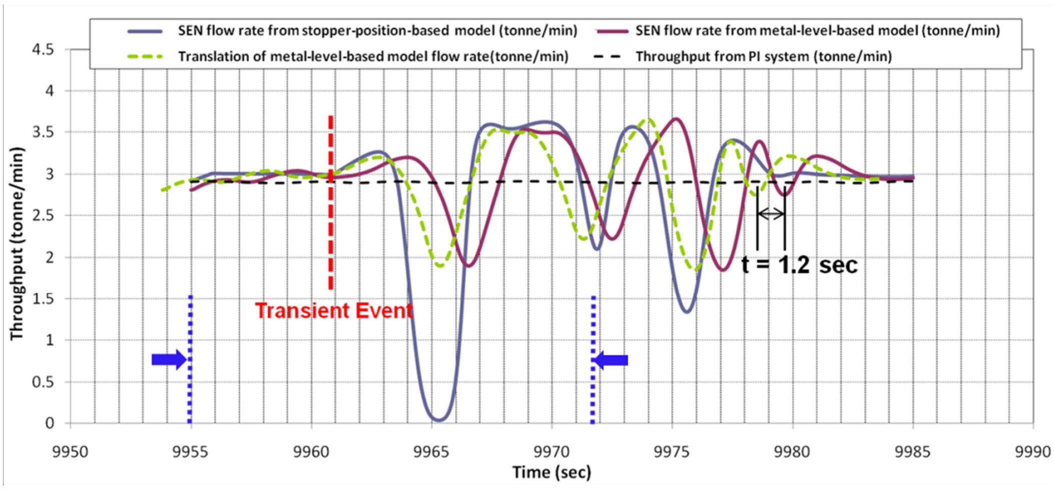

Figure 9. Predicted SEN flow rates from stopper-position-based and metal-level-based model

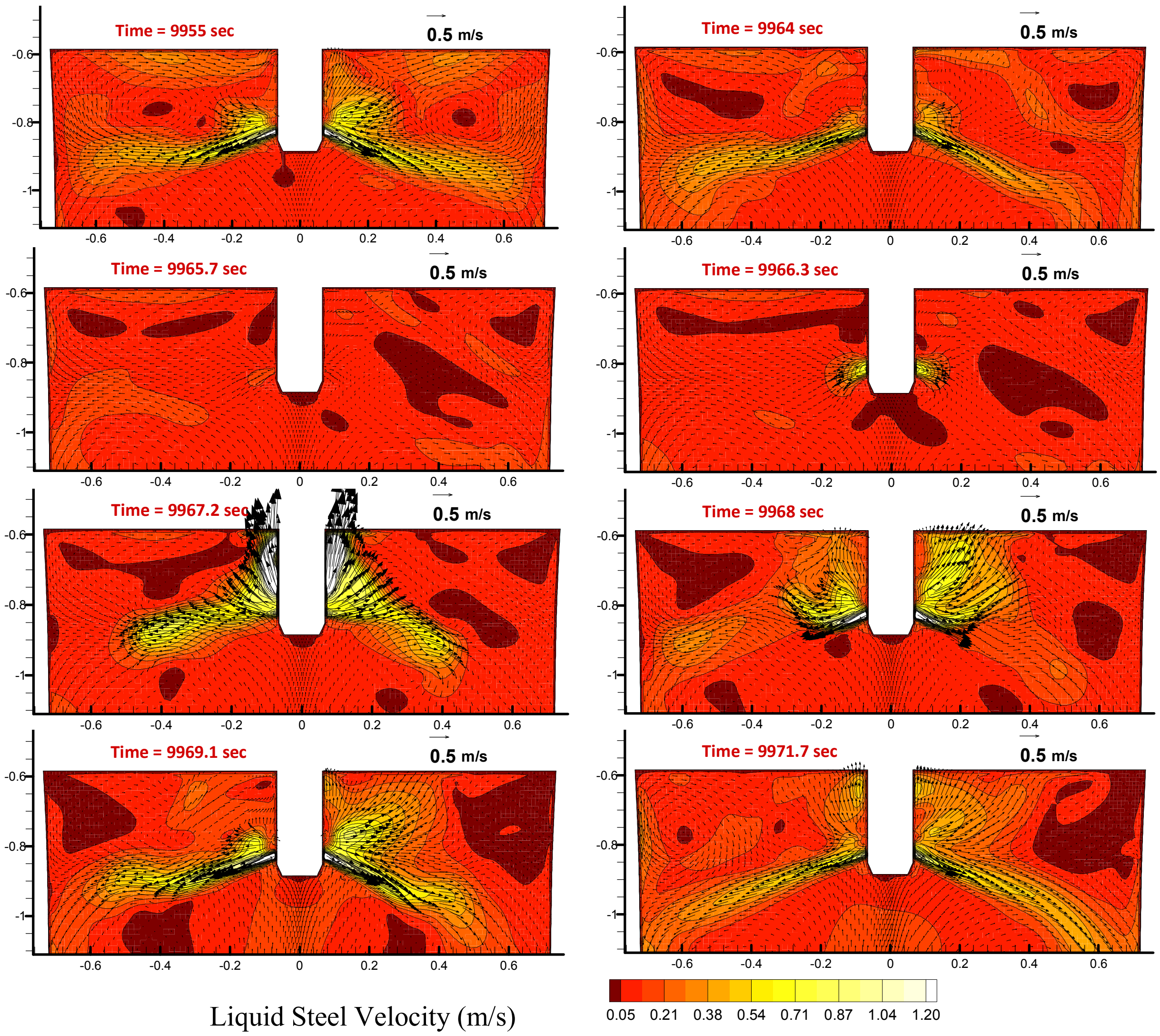

Figure 10. Transient flow patterns during stopper rod movement (axis distances in m)

3.2. Flow pattern evolution during the transient event

Evolution of the flow pattern in the mold simulated during the 16.3sec time interval (indicated with vertical dotted blue lines in Figure 9) of multiple stopper-rod movements is shown in Figure 10. Each frame is plotted at the center plane between broad mold faces. The initial quasi-steady state flow field (at 9955sec) is observed to be a symmetric double-roll flow pattern. As inlet liquid steel flow rate decreases, (eg. at 9964sec), the strength of the jets decreases. Jet strength continues to decrease (9965.7sec) and then starts to recover (at 9966.3sec). Then, (at 9967.2sec), a strong burst of liquid steel shoots up towards the meniscus near the SEN, and significant disturbance of the meniscus is observed, which likely causes liquid slag droplets to get entrained into the liquid pool. This phenomenon is probably caused by the strong buoyancy force from a large amount of rising argon gas. Between time 9968 and 9969.2sec, the upward liquid stream towards meniscus becomes less intensive, and liquid steel jets towards the narrow faces begin to develop, and wobbling of the jets is observed. Finally, at time 9971.7sec, the jet swinging disappears, and the steady flow pattern is re-established.

3.3. Comparison of Predicted and Measured Mold Level

The flow pattern changes caused by the stopper rod movements also affect the mold level profile and cause fluctuations at the top surface, which can be detrimental to steel quality. In this simulation, a flat wall is imposed at the top surface, so to predict mold level, a simple pressure calculation is used:

$$\Delta h = \frac{p - p_0}{\rho_L g} \tag{10}$$

where Δh is the mold level deviation, p is the pressure at top surface, and p_0 is the pressure corresponding to the reference mold level used in determining Δh. ρ_L is the liquid density, and g is the gravitational acceleration. Displacement of the liquid slag layer is neglected in this equation, because the entire layer was judged to be thin enough to simply rise and fall with the steel surface profile variations.

The predicted mold level during the simulated 16.3sec interval with stopper rod movements agrees very well with the measured unfiltered mold level data, at the midway point between SEN and narrow face along the centerline, as shown in Figure 11. Note that there is significant asymmetry between the left and right sides of the mold, owing to chaotic turbulence.

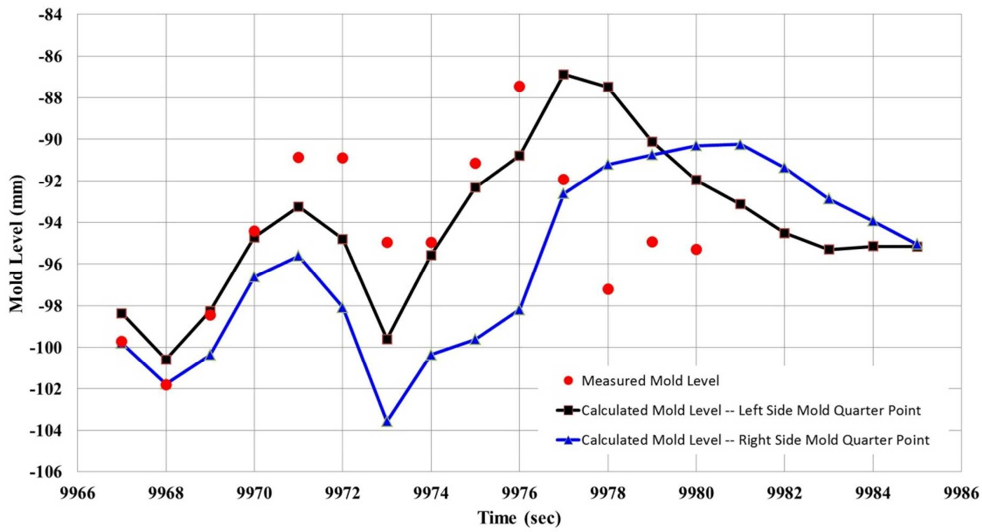

Figure 11. Comparison of calculated and measured mold level

4. Conclusions

A complete system of models is presented in this work to study transient argon-steel two-phase flow in the SEN and mold region during continuous casting process. Each submodel has been validated independently and the following conclusions can be drawn:

1. Gas flow through the hot porous refractory of the nozzle walls is nonuniform and greatly affects the gas flow rate injected into the liquid steel. The porous-flow model presented here is an important tool to determine this flow distribution and to estimate the initial mean bubble size in the nozzle, which are two crucial parameters in liquid-gas two phase flow simulations.
2. Methods such as the stopper-position-based model and the porous-flow model are required to predict the time-dependent flow rates of steel and argon in the nozzle, to provide accurate inlet conditions for transient simulations.
3. Simulated flow during a transient event suggests that significant disturbances of the meniscus occur during stopper rod movements, which may be responsible for slag entrapment leading to formation of sliver defects in the final product.
4. The model system is validated by the match between predicted and measured mold level at the plant.

Acknowledgements

The authors would like to thank the members of the Continuous Casting Consortium in University of Illinois at Urbana-Champaign for their support of our research work, and also to B. Forman at ArcelorMittal Global R&D in East Chicago for his help with the static test. ArcelorMittal Global R&D in Maizières, France is acknowledged for providing the SVC devices for trials. The authors also want to show their gratitude towards S. Chung, M. Trinh and D. Currey at ArcelorMittal Dofasco Inc. in Canada for their kind help with the plant trials.

References

[1] Meng Y and Thomas B G 2003 *Metall. Mater. Trans. B* **34B(5)** 685-705
[2] Hibbeler L and Thomas B G 2010 *Proc. AISTech 2010 Steelmaking Conf.* (Pittsburgh)
[3] Liu R, Sengupta J, Thomas B G *et al* 2011 *Proc. AISTech 2011 Conf.* (Indianapolis) p1619-1631
[4] Liu R, Thomas B G and Sengupta J 2011 *CCC Annual Meeting* (Urbana-Champaign)
[5] Dawe R and Smith E 1969 *Science* **163** 675-676.
[6] FLUENT ANSYS Inc. 2007 *FLUENT 6.3-Manual* (Lebanon, NH)
[7] Lee G, Thomas B G and Kim S 2010 *Met. Mater. Int.* **16(3)** 501-506
[8] Bai H and Thomas B G 2001 *Metal Mater. Trans. B.* **32B(6)** 1143-1159
[9] Schiller L and Naumann Z 1935 *Z. Ver. Deutsch. Ing.* **77** 318
[10] Yuan Q, Thomas B G and Vanka S P 2004 *Metal. Mater. Trans. B.* **35B(4)** 685-702
[11] Liu R, Sengupta J, Thomas B G *et al* 2011 *Proc. TMS 2011 Conf.* (San Diego) p 51-58